SUPPRESSING FLOW-INDUCED VIBRATIONS BY PARAMETRIC EXCITATION

Siti Fatimah*, and Ferdinand Verhulst†

Mathematisch Instituut, University of Utrecht, PO Box 80.010, 3508 TA Utrecht, The Netherlands

ABSTRACT. The possibility of suppressing self-excited vibrations of mechanical systems using parametric excitation is discussed. We consider a two-mass system of which the main mass is excited by a flow-induced, self excited force. A single mass which acts as a dynamic absorber is attached to the main mass and, by varying the stiffness between the main mass and the absorber mass, represents a parametric excitation. It turns out that for certain parameter ranges full vibration cancellation is possible. Using the averaging method the fully non-linear system is investigated producing as non-trivial solutions stable periodic solutions and tori. In the case of a small absorber mass we have to carry out a second-order calculation.

1. INTRODUCTION

In this paper we solve an open problem formulated by Ecker and Tondl [1]; also we analyse their model to discover many interesting bifurcational phenomena.

Suppressing flow-induced vibrations by using a conventional spring-mass absorber system has often been investigated and applied in practice. It is also well-known that self-excited vibrations can be suppressed by using different kinds of damping, see [2] and [3]. However, only little attention has been paid to vibration suppression by using interaction of different types of excitation.

In the monograph by Tondl [4], some results on the investigation of synchronization phenomena by means of parametric resonances have lead to the idea to apply a parametric excitation for suppressing self-excited vibrations. The conditions for full vibration suppression (also called quenching) were formulated first in [5] and [6].

Using the Harmonic Balance Method (see [7]and [8]) in Ecker and Tondl [1] a two-mass system is studied; see Figure 1. The main mass is excited by a flow-induced, self-excited force, in which the self-excitation is of Rayleigh type. This mass is connected to the absorber mass by a linear spring. The connecting stiffness between two masses is a harmonic function of time and represents a parametric excitation. The analysis in [1] shows that the interval of self-excitation can exist in the vinicity of the combination resonance $\eta = \Omega_2 - \Omega_1$, where Ω_1 and Ω_2 are the natural frequencies of the linearized system without damping and η is the parametric excitation frequency. There are two conditions for suppressing self-excited vibrations. The first condition involves the overall damping of the system. The second one is related to the parametric excitation frequency. It determines whether full quenching can be achieved or not in a certain interval. In general only a few frequency ratios can be used to obtain the necessary parametric resonance; see for instance [[1],[2],[4],[8]].

*fatimah@math.uu.nl, on leave from the Mathematics dept. of FMIPA, Education University of Indonesia (UPI), Bandung, Indonesia.

†verhulst@math.uu.nl

A numerical investigation of the fully non-linear system in [1] shows that the contribution of the parametric excitation can be predicted correctly by their first order approximative analysis only for values of the mass ratio $M \geq 0.1$. We will show that for smaller mass ratio we have to re-scale the system and a higher order approximation will be necessary to obtain more accurate results for lower values of the mass ratio.

In this paper the same system as in [1] is considered; the model is described in section 2. We will use the averaging method and numerical bifurcation techniques to study the system. The first order approximation is used to analyze the conditions for full vibration suppression in section 4-6. It turns out that full vibration cancellation is possible in an open parameter set. This is illustrated analytically. In section 7 and 8 we study what happens when vibration cancellation does not take place. It turns out that several Hopf bifurcations are possible, producing periodic solutions. Also Neimark-Sacker bifurcations arise which produce stable tori with relative high amplitudes. Finally, in section 9 we return to the realistic problem of a small absorber mass. A second-order approximation has to be calculated in this case with as a result that, although full vibration cancellation is impossible, a fairly large part of vibration quenching can be achieved.

2. The Model

Our study is based on a model for the suppression of flow-induced vibrations by a dynamic absorber with parametric excitation formulated in [1]. Consider a two-mass system consisting of a main mass m_2 which is in flow-induced vibration and an absorber mass m_1 which is attached to the main mass by a spring-damper element, see Figure 1. The elastic mounting $k(t)$ of the absorber mass is a combination of a spring and a device operating such that the stiffness $k(t)$ is changed periodically. Damping is represented by the linear viscous damper c_1. The main mass m_2 is supported by a spring with constant stiffness k_2; it has a linear viscous damper with damping parameter c_2. In actual constructions one usually has $m_1 < m_2$.

A flow-generated self-excited force is acting on the main mass m_2 with critical flow velocity U_c and a limited vibration amplitude in the over-critical region; as usual it is represented by a Rayleigh force.

The displacements of mass m_1 and mass m_2 are denoted by the coordinates y_1 and y_2, respectively. The variation of the stiffness of the absorber element is supposed to be a harmonic function with a small amplitude.

This system is represented by the following nonlinear equations of motion

$$
\begin{aligned}
& m_1 y_1'' + c_1(y_1' - y_2') + \\
& \qquad + k_1(1 + \varepsilon \cos\omega\tau)(y_1 - y_2) = 0, \\
& m_2 y_2'' - c_1(y_1' - y_2') + \\
& \qquad - k_1(1 + \varepsilon \cos\omega\tau)(y_1 - y_2) + c_2 y_2' + k_2 y_2 - b_\circ U^2(1 - \gamma_\circ {y_2'}^2) y_2' = 0.
\end{aligned} \tag{2.1}
$$

where ε is a small positive parameter, $0 < \varepsilon << 1$.

In the decoupled system, where we only consider vibrations of the main mass m_2, self-excited vibrations occur if $c_2 - b_\circ U^2 < 0$.

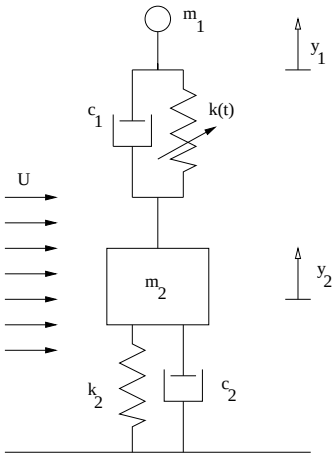

FIGURE 1. System consisting of a flow-excited main mass m_2 and a vibration absorber m_1 with time-dependent connecting stiffness $k(t)$.

3. TRANSFORMATION OF THE SYSTEM TO A STANDARD FORM

Dimensionless coordinates x_j can be defined with respect to a given reference value $y_\circ$:

$$x_j = y_j/y_\circ \qquad j = 1, 2, \tag{3.1}$$

By introducing the characteristic parameters of the system

$$\bar{\omega}^2 = \frac{k_1}{m_1} \quad , \quad {\omega_\circ}^2 = \frac{k_2}{m_2} \quad , \quad \eta = \frac{\omega}{\omega_\circ} \quad , \quad Q^2 = \frac{\bar{\omega}^2}{{\omega_\circ}^2}, \tag{3.2}$$

and by using the time-transformation

$$\omega_\circ t = \tau, \tag{3.3}$$

the following dimensionless form of system (2.1) is obtained

$$\begin{aligned} &x_1'' + \kappa_1(x_1' - x_2') + \\ &\quad + Q^2(1 + \varepsilon\cos\eta\tau)(x_1 - x_2) = 0, \\ &x_2'' - M\kappa_1(x_1' - x_2') + \\ &\quad - MQ^2(1 + \varepsilon\cos\eta\tau)(x_1 - x_2) + \kappa_2 x_2' + x_2 - \beta V^2(1 - \gamma {x_2'}^2)x_2' = 0. \end{aligned} \tag{3.4}$$

where

$$\begin{aligned} \kappa_1 = \frac{c_1}{m_1\omega_\circ} \quad , \quad \kappa_2 = \frac{c_2}{m_2\omega_\circ} \quad , \quad \beta = \frac{b_\circ {U_\circ}^2}{m_2\omega_\circ} \\ V^2 = \frac{U^2}{{U_\circ}^2} \quad , \quad \gamma = \gamma_\circ {\omega_\circ}^2 \quad , \quad M = \frac{m_1}{m_2}. \end{aligned} \tag{3.5}$$

Parameter $U_\circ$ is a chosen reference value for the flow velocity. When $U_\circ$ reaches the critical flow velocity $U_c = \sqrt{c_2/b_\circ}$, the relative critical flow velocity is $V_c = 1$.

In order to transform the system into a standard form and to make the size of the parameters more explicit, we scale $\kappa_{1,2} = \varepsilon\bar{\kappa}_{1,2}$, and $\beta = \varepsilon\bar{\beta}$ while assuming that the other parameters are $O(1)$ with respect to ε. However, in quite a number of applications the absorber mass m_1 will be small with respect to the main mass m_2; we shall return to this case in section 9. If $\varepsilon = 0$, the linear parts of (3.4) now depend on the mass ratio M and the frequency ratio Q. Note, that if $\varepsilon > 0$, three frequencies play a part. Using the linear transformation

$$\begin{aligned} x_1 &= \bar{x}_1 + \bar{x}_2, \\ x_2 &= a_1\bar{x}_1 + a_2\bar{x}_2. \end{aligned} \tag{3.6}$$

leads to the standard form

$$\begin{aligned} \bar{x}_1'' + \Omega_1^2\bar{x}_1 &= -\frac{\varepsilon}{a_1 - a_2}F_1(\bar{x}_1, \bar{x}_1', \bar{x}_2, \bar{x}_2', \eta\tau), \\ \bar{x}_2'' + \Omega_2^2\bar{x}_2 &= -\frac{\varepsilon}{a_1 - a_2}F_2(\bar{x}_1, \bar{x}_1', \bar{x}_2, \bar{x}_2', \eta\tau), \end{aligned} \tag{3.7}$$

where the natural frequencies of the linearized system without damping and for $\varepsilon = 0$, Ω_1 and Ω_2, are

$$\Omega_{1,2}^2 = 1/2\left(1 + Q^2(1+M)\right) \mp \sqrt{1/4(1+Q^2(1+M))^2 - Q^2} \tag{3.8}$$

and $a_{1,2}$ satisfy the relations

$$Q^2a_j^2 + (MQ^2 + 1 - Q^2)a_j - Q^2M = 0, \quad (j = 1, 2) \tag{3.9}$$

from which follows

$$a_{1,2} = \frac{1}{Q^2}\left(\frac{1}{2}(-MQ^2 - 1 + Q^2) \pm \sqrt{\frac{1}{4}(MQ^2 + 1 + Q^2)^2 - Q^2}\right). \tag{3.10}$$

Note that the functions F_1 and F_2 (system (3.7)) are depending on the parametric excitation frequency η, and that the following conditions hold

$$\Omega_2 > \Omega_1, \quad a_1a_2 = -M, \quad 0 < a_1 < 1, \quad \text{and} \quad a_2 < -M. \tag{3.11}$$

4. The Normal Form by Averaging

We will use the method of averaging to study the system near the *combination resonance* $\Omega_2 - \Omega_1 = \eta_\circ$. Transforming $t \to \eta\tau$ and allowing detuning near $\eta_\circ$ by putting

$$\eta = \eta_\circ + \varepsilon\bar{\sigma}. \tag{4.1}$$

system (3.7) becomes to first order in ε

$$\begin{aligned} \ddot{\bar{x}}_1 + \omega_1^2\bar{x}_1 &= -\frac{\varepsilon}{(a_1 - a_2)\eta_\circ^2}\bar{F}_1(\bar{x}_1, \dot{\bar{x}}_1, \bar{x}_2, \dot{\bar{x}}_2, t), \\ \ddot{\bar{x}}_2 + \omega_2^2\bar{x}_2 &= -\frac{\varepsilon}{(a_1 - a_2)\eta_\circ^2}\bar{F}_2(\bar{x}_1, \dot{\bar{x}}_1, \bar{x}_2, \dot{\bar{x}}_2, t). \end{aligned} \tag{4.2}$$

where $\omega_{1,2} = \frac{\Omega_{1,2}}{\eta_\circ}$ and

(4.3)

$$\begin{aligned} \bar{F}_1 &= -2(a_1 - a_2)\omega_1\Omega_1\bar{\sigma}\bar{x}_1 + \theta_{11}\eta_\circ\dot{\bar{x}}_1 + \theta_{12}\eta_\circ\dot{\bar{x}}_2 - (Q_{11}\bar{x}_1 + Q_{12}\bar{x}_2)\cos t + B\eta_\circ^3(a_1\dot{\bar{x}}_1 + a_2\dot{\bar{x}}_2)^3 \\ \bar{F}_2 &= -2(a_1 - a_2)\omega_2\Omega_2\bar{\sigma}\bar{x}_2 + \theta_{21}\eta_\circ\dot{\bar{x}}_1 + \theta_{22}\eta_\circ\dot{\bar{x}}_2 - (Q_{21}\bar{x}_1 + Q_{22}\bar{x}_2)\cos t - B\eta_\circ^3(a_1\dot{\bar{x}}_1 + a_2\dot{\bar{x}}_2)^3 \end{aligned}$$

$$
\begin{aligned}
Q_{12} &= Q^2(a_2+M)(1-a_2) && (4.4)\\
Q_{21} &= -Q^2(a_1+M)(1-a_1) && (4.5)\\
\theta_{11} &= -\bar{\kappa}_1(a_2+M)(1-a_1)+a_1(\bar{\kappa}_2-\bar{\beta}V^2) && (4.6)\\
\theta_{22} &= \bar{\kappa}_1(a_1+M)(1-a_2)-a_2(\bar{\kappa}_2-\bar{\beta}V^2) && (4.7)\\
B &= \bar{\beta}V^2\gamma && (4.8)
\end{aligned}
$$

To study the behavior of the solutions, we transform

$$
\begin{aligned}
\bar{x}_1 &= u_1\cos\omega_1 t+v_1\sin\omega_1 t, \quad \dot{\bar{x}}_1 = -\omega_1 u_1\sin\omega_1 t+\omega_1 v_1\cos\omega_1 t\\
\bar{x}_2 &= u_2\cos\omega_2 t+v_2\sin\omega_2 t, \quad \dot{\bar{x}}_2 = -\omega_2 u_2\sin\omega_2 t+\omega_2 v_2\cos\omega_2 t.
\end{aligned} \tag{4.9}
$$

This transformation is useful when studying the stability of the trivial solution of system (4.2); stability implies the possibility of vibration cancellation. In later sections the polar coordinate transformation will be useful for studying non-trivial solutions. After averaging over 2π and then rescaling time through $\frac{\varepsilon}{2(a_1-a_2)\eta_\circ^2}$, we obtain the normal form

$$
\begin{aligned}
\dot{u_1} &= -\theta_{11}\eta_\circ u_1-2(a_1-a_2)\Omega_1\bar{\sigma}v_1-\frac{1}{2}\frac{Q_{12}}{\omega_1}v_2-\frac{3}{2}{\eta_\circ}^3 Bu_1\left(\frac{1}{2}\omega_1^2a_1^3(u_1^2+v_1^2)+\omega_2^2a_1a_2^2(u_2^2+v_2^2)\right),\\
\dot{v_1} &= 2(a_1-a_2)\Omega_1\bar{\sigma}u_1-\theta_{11}\eta_\circ v_1+\frac{1}{2}\frac{Q_{12}}{\omega_1}u_2-\frac{3}{2}{\eta_\circ}^3 Bv_1\left(\frac{1}{2}\omega_1^2a_1^3(u_1^2+v_1^2)+\omega_2^2a_1a_2^2(u_2^2+v_2^2)\right),\\
\dot{u_2} &= -\frac{1}{2}\frac{Q_{21}}{\omega_2}v_1-\theta_{22}\eta_\circ u_2-2(a_1-a_2)\Omega_2\bar{\sigma}v_2+\frac{3}{2}{\eta_\circ}^3 Bu_2\left(a_1^2a_2\omega_1^2(u_1^2+v_1^2)+\frac{1}{2}a_2^3\omega_2^2(v_2^2+u_2^2)\right),\\
\dot{v_2} &= \frac{1}{2}\frac{Q_{21}}{\omega_2}u_1+2(a_1-a_2)\Omega_2\bar{\sigma}u_2-\theta_{22}\eta_\circ v_2+\frac{3}{2}{\eta_\circ}^3 Bv_2\left(a_1^2a_2\omega_1^2(u_1^2+v_1^2)+\frac{1}{2}a_2^3\omega_2^2(v_2^2+u_2^2)\right)
\end{aligned} \tag{4.10}
$$

where we use again the dot to indicate derivation with respect to the re-scaled time.

System (4.10) can be reduced to the three-dimension system by transforming the system using the following transformation,

$$
u_i = -R_i\cos\psi_i, \quad \text{and} \quad v_i = R_i\sin\psi_i, \quad i=1,2, \tag{4.11}
$$

to transform system (4.10) to

$$
\begin{aligned}
\dot{R}_1 &= -\theta_{11}\eta_\circ R_1-\frac{1}{2}\frac{Q_{12}}{\omega_1}R_2\sin\Psi-\frac{3}{4}{\eta_\circ}^3 Ba_1^3\omega_1^2R_1^3-\frac{3}{2}{\eta_\circ}^3 Ba_1a_2^2\omega_2^2R_1R_2^2\\
\dot{R}_2 &= -\theta_{22}\eta_\circ R_2+\frac{1}{2}\frac{Q_{21}}{\omega_2}R_1\sin\Psi+\frac{3}{4}{\eta_\circ}^3 Ba_2^3\omega_2^2R_2^3+\frac{3}{2}{\eta_\circ}^3 Ba_1^2a_2\omega_1^2R_2R_1^2\\
\dot{\Psi} &= 2(a_1-a_2)\eta_\circ\bar{\sigma}+\left(\frac{1}{2}\frac{Q_{21}}{\omega_2}\frac{R_1}{R_2}+\frac{1}{2}\frac{Q_{12}}{\omega_1}\frac{R_2}{R_1}\right)\cos\Psi
\end{aligned} \tag{4.12}
$$

where $\Psi=\psi_2-\psi_1$ and $R_i=\sqrt{u_i^2+v_i^2}$, $i=1,2$. Note that fixed points we will find in system (4.12) correspond with periodic solutions of system (4.10). We also obtain the normal form system (4.12) by directly introducing the polar coordinate transformation $\bar{x}_i=R_i\cos(\omega_i t+\psi_i)$ and $\dot{\bar{x}}_i=-R_i\cos(\omega_i t+\psi_i)$ $(i=1,2)$ to transform system (4.2) and average it over 2π, rescaling time by $\frac{\varepsilon}{2(a_1-a_2)\eta_\circ^2}$.

5. Conditions for Vibration Cancellation:Linear Case

In [3,6,8] systems have been studied involving interaction of self-excitation and parametric excitation. In the methods used there an implicit assumption on the magnitude of the parameters corresponds with our assumptions in the preceding section; in section 9 this will change. Here we present an independent analysis of the stability of the trivial solution based on the averaged normal form (4.10).

The linearization of averaged system (4.10) at the trivial solution has the form

$$\begin{pmatrix} -\theta_{11}\eta_\circ & -2(a_1-a_2)\Omega_1\bar{\sigma} & 0 & -\frac{1}{2}\frac{Q_{12}}{\omega_1} \\ 2(a_1-a_2)\Omega_1\bar{\sigma} & -\theta_{11}\eta_\circ & \frac{1}{2}\frac{Q_{12}}{\omega_2} & 0 \\ 0 & -\frac{1}{2}\frac{Q_{21}}{\omega_2} & -\theta_{22}\eta_\circ & -2(a_1-a_2)\Omega_2\bar{\sigma} \\ \frac{1}{2}\frac{Q_{21}}{\omega_2} & 0 & -2(a_1-a_2)\Omega_2\bar{\sigma} & -\theta_{22}\eta_\circ \end{pmatrix}. \tag{5.1}$$

where its characteristic equation can be expressed as

$$\lambda^4 + q_1\lambda^3 + q_2\lambda^2 + q_3\lambda + q_4 = 0, \tag{5.2}$$

in which q_1, q_2, q_3 and q_4 are depended on the parameters. Note that we have $Q_{12} < 0$ and $Q_{21} < 0$. The linear damping coefficients θ_{11} and θ_{22} have a positive sign if $\bar{\beta}V^2 - \bar{\kappa}_2 < 0$; in this case there is no self-excitation. In the case of self-excitation $\bar{\beta}V^2 - \bar{\kappa}_2 > 0$, there are three conditions for θ_{11} and θ_{22}: $\theta_{11} < 0$ and $\theta_{22} > |\theta_{11}|$, $\theta_{22} < 0$ and $\theta_{11} > |\theta_{22}|$, and both of θ_{22} and θ_{11} are positive.

The signs of the linear damping coefficients θ_{11} and θ_{22} are important to determine conditions when the vibrations can be suppressed. At the boundaries $\theta_{11} = 0$ and $\theta_{22} = 0$ from (3.10), (4.7), and (4.8), we have

$$Q_i \equiv Q = \sqrt{\frac{c_i}{M + (1-M)c_i - c_i^2}}, \quad (i = 1, 2). \tag{5.3}$$

where Q_1 corresponds to $\theta_{11} = 0$ and Q_2 to $\theta_{22} = 0$. The value of c_i is depending on $\bar{\kappa}_{1,2}$, $\bar{\beta}$, and V.

In Figure 2 and Figure 3 we show the boundaries when the θ_{11} and θ_{22} change sign. For numerical calculations we use the parameter sets, from [8] as listed in Table 1.

Table 1: Parameter values for numerical examples.

Parameter	Set I	Set II
ϵ	0.1	0.2
κ_1	0.1	0.2
κ_2	0.1	0.1
β	0.1	0.2
V	$\sqrt{2.1}$	$\sqrt{2.1}$
γ	4	4

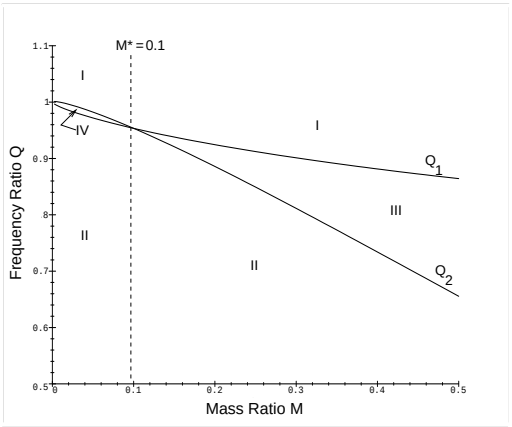

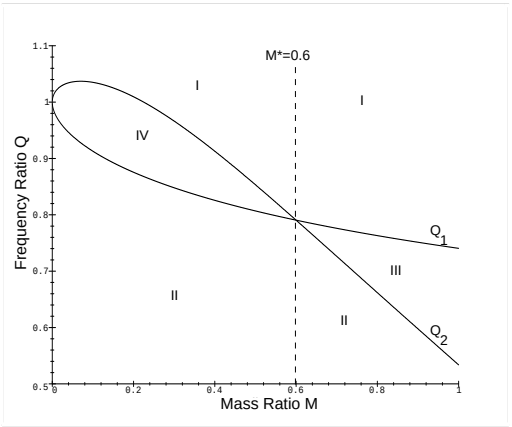

(a) (b)

FIGURE 2. Boundaries of θ_{11} and θ_{22} in the (M, Q)-plane for Parameter Set I , see Table 1. The curves Q_1 and Q_2 correspond with $\theta_{11} = 0$ and $\theta_{22} = 0$, respectively. Region I, $\theta_{11} < 0$ and $\theta_{22} > 0$. Region II, $\theta_{11} > 0$ and $\theta_{22} < 0$. Region III, both θ_{11} and θ_{22} are positive. On the right side of the line $M^\star = 0.1$, $\theta_{11} + \theta_{22} > 0$ and $\theta_{11} + \theta_{22} < 0$ on the left side. (a) For Parameter Set I, (b) for Parameter Set II, see Table 1.

Applying the Routh-Hurwitz criterion to get conditions when the real parts of the eigenvalues of (5.1) have a negative sign leads to two conditions that must be met. The first condition of the Routh-Hurwitz criterion gives

$$\theta_{11} + \theta_{22} > 0. \tag{5.4}$$

The second condition gives the relation

$$p_1 \bar{\sigma}^4 + p_2 \bar{\sigma}^2 + p_3 > 0 \tag{5.5}$$

where p_j, $j = 1, 2, 3$ depend on Q, M, if the other parameters are fixed . Solving at the boundary, we obtain

$$\bar{\sigma}_i = \pm \frac{1}{4} \frac{\theta_{11} + \theta_{22}}{(a_1 - a_2)} \sqrt{-\frac{4\Omega_1\Omega_2\theta_{11}\theta_{22} + Q_{12}Q_{21}}{\Omega_1\Omega_2\theta_{11}\theta_{22}}}, \qquad i = 1, 2. \tag{5.6}$$

where the others two roots are always imaginary. To obtain real values of $\bar{\sigma}_i$ we have the condition $4\Omega_1\Omega_2\theta_{11}\theta_{22} + Q_{12}Q_{21} > 0$ and either θ_{11} or θ_{22} are not negative simultaneously. In the case both of them are positive, the second condition (5.5) is always satisfied.

Furthermore, we obtain

$$M^\star = \frac{(\bar{\beta} V^2 - \bar{\kappa_2}) - \bar{\kappa_1}}{\bar{\kappa_1}} < M \tag{5.7}$$

that is related to condition (5.4).

Substituting equation (5.6) into (4.1), the interval of stability of the trivial solution is determined by

$$\eta_0 + \epsilon\bar{\sigma}_2 < \eta < \eta_0 + \epsilon\bar{\sigma}_1 \tag{5.8}$$

6. Stability of The Trivial Solution

The parametric excitation is used in the case when self-excited vibrations occur. In the coupled system the effectiveness depends on conditions of the parameter damping θ_{11} or θ_{22}. When both of θ_{11} and θ_{22} are positive, this represents the case where the dynamic absorber successfully cancels the self-excited vibration. This happens in region III in Figure 2 (a) and Figure 2 (b).

In Figure 2, within the small area IV to the left of line $M = M^\star$, both of θ_{11} and θ_{22} are negative. There we have that self-excitation is dominant and full vibration quenching is not possible at all. The condition (5.4) is satisfied on the right side of the line $M = M^\star$.

In Figures 3 and 4 we show the instability boundaries of the trivial solution in the (η, Q)-plane for fixed M. These figures represent the instability boundary for parameter Set I and Set II, see Table 1. They show the same characteristic shape of the region of full vibration suppression. One can recognize an overlap of area that stretches along the combination resonance $\eta = \eta_0 + \sigma$ and another area that is independent of the parameter excitation frequency η. Inside the curves we find the trivial solution is stable and unstable outside. Within the area independent of η, vibration cancellation is not caused by the parametric excitation, but the stretching of the area along the anti-resonance curve is caused by the parametric excitation.

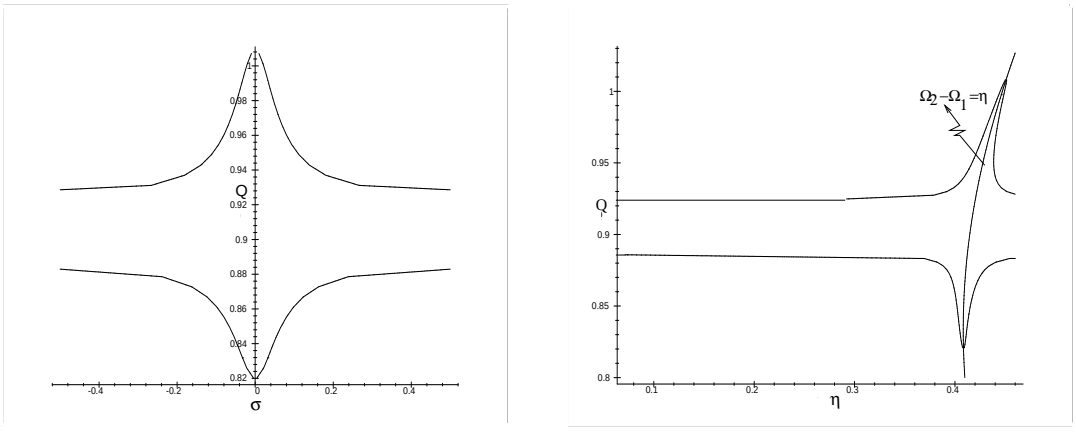

(a) (b)

Figure 3. Stability boundaries for Parameter Set I and fixed $M = 0.2$. (a) In the $(\bar{\sigma}, Q)$-plane, (b) in the (η, Q)-plane. Inside the curves in (a) and (b) the trivial solution is stable (full vibration suppression) and it is unstable outside.

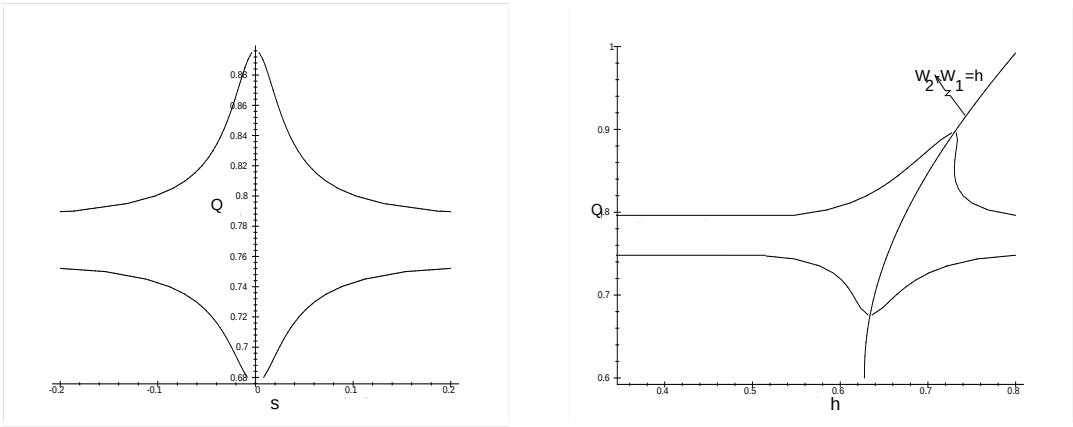

(a) (b)

FIGURE 4. Stability boundaries for Parameter Set II and fixed $M = 0.65$. (a) In the $(\bar{\sigma}, Q)$-plane, (b) in the (η, Q)-plane. Inside the curves in (a) and (b) the trivial solution is stable (full vibration suppression) and it is unstable outside.

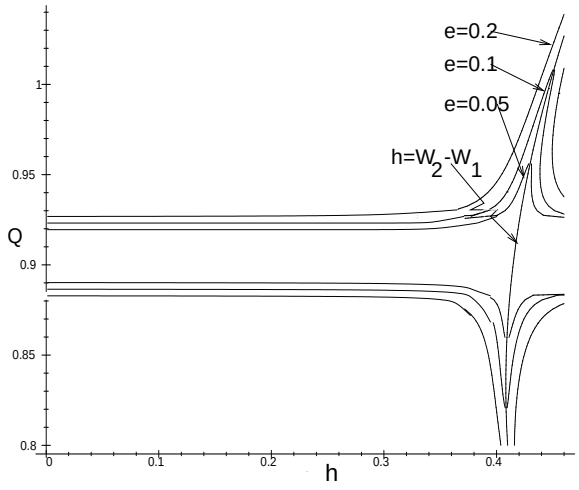

FIGURE 5. Stability boundaries of the trivial solution in the (η, Q)-plane for Parameter set I (see Table 1) for fixed values of the parameter and varying ε and $M = 0.2$.

Note that the region of full vibration suppression in Figure 3 and Figure 4 depends on the mass ratio M. The excitation frequency η has a wider range than the frequency ratio Q.

Near the combination resonance $\eta = \eta_\circ$ or $\sigma = 0$, the enlargement is increasing with higher values of M, but it does not increase proportionally with η.

Figure 5 shows the influence of the amplitude ε of the parametric excitation on the suppressing area. The parameter mainly influences the size of the area near the combination resonance $\eta = \Omega_2 - \Omega_1$. The area of suppressing increases with increasing amplitude ε, indicating that ε is a very effective parameter to obtain a large area of vibration suppression.

We point out that this study of stability of system (4.2) is for the realistic case of mass ratio M smaller than 1. For a fixed value of M in this interval we obtain the shapes along the combination resonance and the area as shown in Figure 3 and Figure 4. In the numerical simulation shown in [8], this area along the combination resonance is splitting up for small M. In section 9 we explain this analytically by a second order approximation.

7. Bifurcations of the trivial solution

In section 6 we have studied the stability of the trivial solution of system (4.10) for a fixed value of $\kappa_1 = 0.1$. We will vary the damping parameter $\theta_{11}(\theta_{22})$ by varying $\kappa_1 \to 0$ and fixing the other parameters to study the bifurcations of the trivial solution leading to periodic solutions and an attracting torus. To study the dynamics of the system near the trivial solution, it is appropriate to use system (4.10). The equivalent system (4.12) in polar coordinates will be used to study the behavior of solutions away from the trivial solution in section 8.

In Figure 6, we present the parameter diagram in the $(\kappa_1, \bar{\sigma})$-plane for Parameter Set I and fixed $Q = 0.95$. The curves $\bar{\sigma}_1$ and $\bar{\sigma}_2$ represent Hopf bifurcation curves of the trivial-solution $\mathbf{X}_\circ$ of system (4.10). The curves are obtained from equation (5.6). Figure 13 (discussed again in section 8) illustrates qualitatively the bifurcation diagram of the trivial solution of system (4.10) in for varying κ_1. Fixing $\bar{\sigma}_1 = 0.1$, we find that the hyperbolic trivial-solution $\mathbf{X}_\circ$ is stable for $\kappa_1 > \kappa_{11}$ and unstable for $\kappa_1 < \kappa_{11}$. The stable trivial solution $\mathbf{X}_\circ$ undergoes Hopf bifurcation at point H_1 then a stable periodic solution $\mathbf{X_1}$ emerges. For fixed value κ_1 in the interval $\kappa_{12} < \kappa_1 < \kappa_{11}$ the real parts of the eigenvalues of the trivial solution $\mathbf{X}_\circ$ which correspond with the vector field (u_1, v_1), are negative. The other two, corresponding with the vector field (u_2, v_2) are negative; they become positive for $\kappa_1 < \kappa_{12}$. We have again Hopf bifurcation at H_2 for the value $\kappa_1 = \kappa_{12}$ and an unstable periodic solution $\mathbf{X_2}$ emerges. Using the continuation program CONTENT [9], we can indicate the appearance of a stable periodic solution $\mathbf{X_1}$. It becomes unstable at $\kappa_1 = \kappa_{13}$ and a stable torus emerges via a Neimark-Sacker bifurcation. We note that the torus occurs in the interval $\kappa_{14} < \kappa_1 < \kappa_{13}$, where $\kappa_{11} = 0.09936$, $\kappa_{12} = 0.08675$, $\kappa_{13} = 0.06367$, and $\kappa_{14} = 0.0228011$. The stability of the system (4.10) for $\kappa_1 < \kappa_{14}$ goes to the periodic solution $\mathbf{X_2}$ which becomes stable at that interval.

We write the amplitudes of the solution of system (4.10) corresponding with the (u_i, v_i)-variables as $R_i = \sqrt{u_i^2 + v_i^2}$ where $i = 1, 2$. In section 8 we will discuss more extensively the periodic solutions $\mathbf{X_i}, \mathbf{i = 1, 2}$, and also the appearance of the torus.

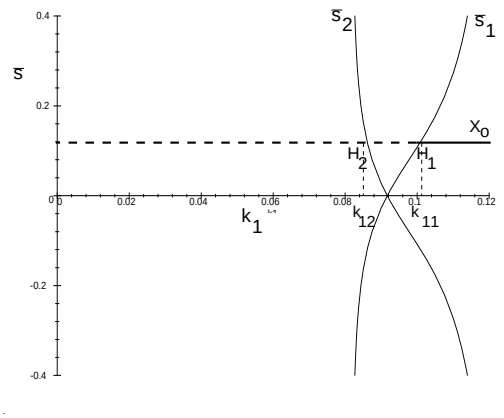

FIGURE 6. The parameter diagram in the $(\kappa_1, \bar{\sigma})$-plane of system (4.10) for Parameter Set I (see Table 1), $M = 0.2$ and $Q = 0.95$. The curves $\bar{\sigma}_i, i = 1, 2.$ indicate Hopf bifurcation curves of the trivial solution $\mathbf{X}_o$. The horizontal line $\bar{\sigma} = 0.1$ is a bifurcation path of the trivial solution. Only for $\kappa_1 > \kappa_{11}$ the trivial solution $\mathbf{X}_o$ is stable. The dashed line indicates the unstable trivial solution and a full line indicates the stable trivial solution . Note that $\kappa_{11} = 0.09936$, $\kappa_{12} = 0.08675$, $\kappa_{13} = 0.06367$, and $\kappa_{14} = 0.0228011$.

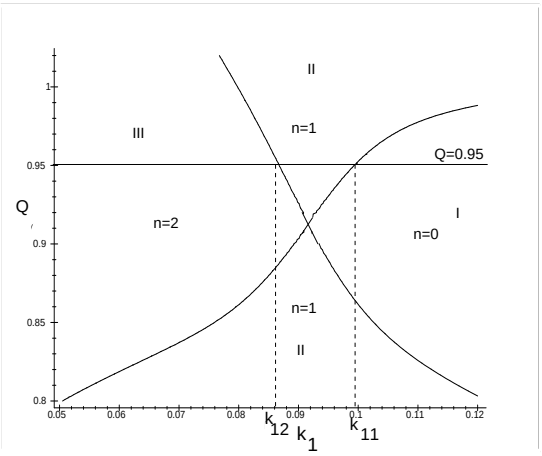

FIGURE 7. Graphical representation of the existence of non-trivial fixed points of system (4.12) in the (κ_1, Q)-plane for Parameter Set I, see Table 1, and for fixed $M = 0.2$. The number of non-trivial periodic solutions is indicated by n. Note that $\kappa_{11} = 0.09936$ and $\kappa_{12} = 0.08675$. The horizontal lines $Q = 0.95$ relate to Figure 11 and Figure 12.

8. Dynamics of the full System

Away from the trivial solution the analysis of the amplitude-phase equations (4.12) is natural and more convenient. Fixed points of this system correspond with periodic solutions (constant amplitudes R_1, R_2, and phase-locked: $\psi_2 - \psi_1$ constant). A Hopf bifurcation of such a fixed point produces a periodic solution of system (4.12) and a torus in the original system. The results are summarized in Figure 10.

8.1. **Existence of the Fixed Points.** Putting $\dot{R}_1 = 0$ and $\dot{R}_2 = 0$ in system (4.12), we find that R_2 is a quadratic function of R_1; the relation is given by $z_1 \equiv f(R_1, R_2) = 0$. From $\dot{R}_1 = 0$ and $\dot{\Psi} = 0$, we have the relation $z_2 \equiv g(R_1, R_2, \bar{\sigma}) = 0$. The curve z_1 in the (R_1, R_2)-plane intersects the R_1-axis or the R_2-axis at the origin, at $(\sqrt{-\frac{4}{3}\frac{\theta_{11}}{Ba_1^3\omega_1^2\eta_o^2}}, 0)$, or $(0, \sqrt{\frac{4}{3}\frac{\theta_{22}}{Ba_2^3\omega_2^2\eta_o^2}})$. Since a_2 is negative, B and a_1 are positive, the curve z_1 will intersect both the R_1-axis and the R_2-axis at nonzero points iff $\theta_{11} < 0$ and $\theta_{22} < 0$. The origin or point $(\sqrt{-\frac{4}{3}\frac{\theta_{11}}{Ba_1^3\omega_1^2\eta_o^2}}, 0)$ is also an intersection of the curve z_2 with those axes. The curve z_2 has two branches parameterized by $\bar{\sigma}$ for $\theta_{11} < 0$, and it has only one branch for $\theta_{11} > 0$.

The fixed points of system (4.12) are obtained by intersecting z_1 and z_2, where $z_1 \cap z_2 = \emptyset$ for $\bar{\sigma}_2 < \bar{\sigma} < \bar{\sigma}_1$ and $\bar{\sigma}_2 < 0$ and $\bar{\sigma}_1 > 0$. The explicit expression for $\bar{\sigma}_i$ $(i = 1, 2)$ can be found from equation (5.6).

Figure 7 shows graphical representations in the (κ_1, Q)-plane of the existence of non-trivial fixed points of system (4.12) for Parameter set I (see Table 1), $\bar{\sigma} = 0.1$ and $M = 0.2$. System (4.12) has no non-trivial fixed point in region I. There is only one non-trivial fixed point $\mathbf{X_1}$ in region II. The non-trivial fixed points $\mathbf{X_1}$ and $\mathbf{X_2}$ exist in region III.

We note that θ_{11} and θ_{22} always have a different sign in region II. Figure 8 and 9 show non-trivial fixed points of system (4.12) for each region in Figure 7. For fixed values $Q = 0.95$ and $\kappa_1 = 0.1$ in region II, the curve z_2 has two branches parameterized by $\bar{\sigma}$, see Figure 8. There is one intersection point between the curve z_1 and z_2 indicated by point $\mathbf{X_1^i}$. In Figure 7, we fixed $Q = 0.8$ and $\kappa_1 = 0.1$ in region II; there is only one branch of the curve z_2, in this case we have $\theta_{11} > 0$ and $\theta_{22} < 0$. Figure 9 illustrates the non-trivial fixed points in region III. For fixed $Q = 1$ and $\kappa_1 = 0.05$, there are two branches of the curve z_2 parameterized by $\bar{\sigma}$ which intersect the curve z_1 at point $\mathbf{X_1^i}$ and point $\mathbf{X_2^i}$.

When we fix $Q = 0.95$, the boundaries of the existence of the non-trivial solution is shown in the $(\kappa_1, \bar{\sigma})$-plane, see Figure 10. The curves $\bar{\sigma}_i, i = 1, 2.$ represent the boundaries of the existence of the non-trivial fixed points $\mathbf{X_1}$ and $\mathbf{X_2}$, respectively. Note that only in the right side of the curve $\bar{\sigma}_1$ the trivial solution is stable. The domains of the region I, II and III are $\bar{\sigma}_1 < \bar{\sigma}$, $\bar{\sigma}_1 < \bar{\sigma} < \bar{\sigma}_2$, and $\bar{\sigma} < \bar{\sigma}_2$, respectively. The curves CH_1 and CH_2 indicate Hopf bifurcation curves of the non-trivial fixed points $\mathbf{X_1}$ and $\mathbf{X_2}$, respectively. These curves are found by using the continuation program CONTENT [9].

Region III is divided by the curves $CH_i, i = 1, 2$ into regions $\mathrm{III_a}$ to $\mathrm{III_e}$. The region $\mathrm{III_a}$ is for $CH_i < \bar{\sigma} < \bar{\sigma}_2, i = 1, 2..$ The region $\mathrm{III_b}$ is for $CH_2 < \bar{\sigma} < CH_1$ or $0 < \bar{\sigma} < CH_1$. The region $\mathrm{III_c}$ is for $0 < \bar{\sigma} < CLP$, region $\mathrm{III_d}$ for $CLP < \bar{\sigma} < CH_i, i = 1, 2.$, and region $\mathrm{III_e}$ for $CH_1 < \bar{\sigma} < CH_2$ or $0 < \bar{\sigma} < CH_2$.

In region I of the Figure 10, there is no non-trivial fixed point of system (4.12). The non-trivial fixed point $\mathbf{X_1}$ exists in region II and III. It is only stable in region II and III_a. The non-trivial fixed point $\mathbf{X_2}$ exists in the region III. It is stable in the region III_c, III_d, and III_e.

The stable non-trivial solution $\mathbf{X_i}$ is indicated by $\mathbf{X_i^+}$ and $\mathbf{X_i^-}$ for the unstable non-trivial solution $\mathbf{X_i}$, $\mathbf{i = 1, 2}$.

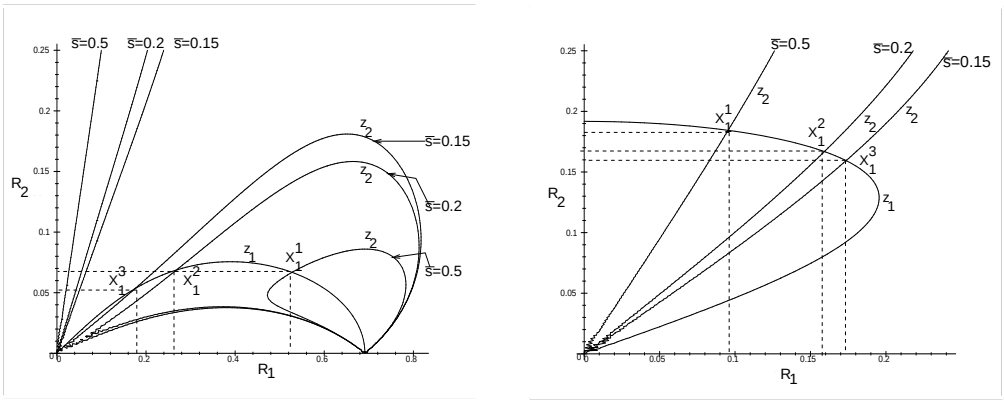

(a) (b)

FIGURE 8. The non-trivial fixed point of system (4.12), for Parameter Set I, see Table 1, $M = 0.2$. (a) For $Q = 0.95$ and $\kappa_1 = 0.1$ in region II Figure 7, there is a single fixed point $\mathbf{X_1^i}$ shown by the intersection of two curves z_1 and z_2 (parameterized by $\bar{\sigma}$). (b) For fixed $Q = 0.8$ and $\kappa_1 = 0.1$ in region II, there is a single fixed point $\mathbf{X_1^i}$ shown by the intersection of two curves z_1 and z_2 (parameterized by $\bar{\sigma}$).

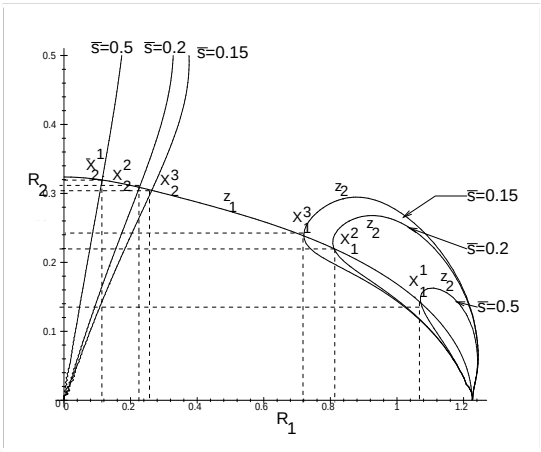

FIGURE 9. The non-trivial fixed point of system (4.12), for Parameter Set I, see Table 1, $M = 0.2$. For fixed $Q = 1$ and $\kappa_1 = 0.05$ in region III, there are two fixed points $\mathbf{X_1^i}$ and $\mathbf{X_2^i}$ shown by the intersection of two curves z_1 and z_2 (two branches parameterized by $\bar{\sigma}$)

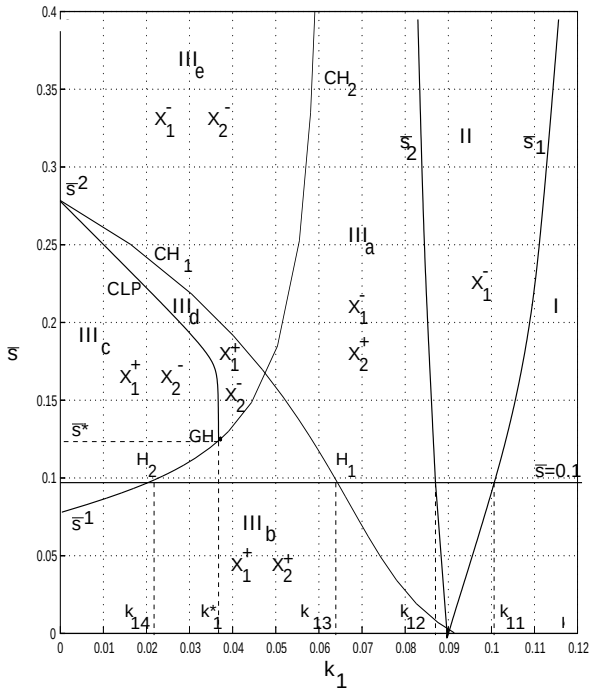

FIGURE 10. The parameter diagram of system (4.12) in the $(\kappa_1, \bar{\sigma})$-plane, for Parameter Set I, see Table 1, $M = 0.2$ and $Q = 0.95$. The curves $\bar{\sigma}_i, i = 1, 2.$ give the boundaries of the existence of the fixed points $\mathbf{X_1}$ and $\mathbf{X_2}$, respectively. $\mathbf{X_i^+}$ indicates a stable non-trivial fixed point $\mathbf{X_i}$ and $\mathbf{X_i^-}$ indicates an unstable one for $\mathbf{i = 1, 2}$. The curves $CH_i, i = 1.2$ indicate Hopf bifurcation curves of the non-trivial fixed points $\mathbf{X_1}$ and $\mathbf{X_2}$, respectively. As these fixed points correspond with periodic solutions, the curves CH_1 represent Neimark-Sacker bifurcation of the original system. The point GH at $\kappa_1 = \kappa_1^* = 0.046897$ and $\bar{\sigma} = \bar{\sigma}^* = 0125067$ indicates an interchange point of the supercritical Hopf bifurcation and the subcritical Hopf bifurcation of the non-trivial fixed point $\mathbf{X_2}$. Note that for $\bar{\sigma} > \bar{\sigma}^*$ the bifurcation is subcritical, and it is supercritical for $\bar{\sigma} < \bar{\sigma}^*$. The horizontal line $\bar{\sigma} = 0.1$ is an example of a bifurcation path of the solutions of system 4.12. The curve CLP represents a limit point bifurcation curve of the periodic solution $\mathbf{Ps}$ which appears via a Hopf bifurcation at curve CH_1. Crossing this curve the stable periodic solution $\mathbf{Ps}$ vanishes. Note that $\bar{\sigma}^2 = 0.07769$, $\bar{\sigma}^1 = 0.279403$, $\kappa_{11} = 0.09936$, $\kappa_{12} = 0.08675$, $\kappa_{13} = 0.06367$, and $\kappa_{14} = 0.0228011$.

8.2. **Bifurcations: Periodic Solutions and an Attracting Torus.** Applying the continuation program CONTENT [9] we obtain the stability diagram of the non-trivial fixed point $\mathbf{X_1}$ of system (4.12) for Parameter Set I (fixed $M = 0.2$ and $Q = 0.95$) in the $(\bar{\sigma}, R_1)$ and $(\bar{\sigma}, R_2)$ planes, see Figure 11. The illustrations are obtained by varying $\bar{\sigma}$ along line $Q = 0.95$, see Figure 3 (a) in section 6 for the diagram parameter in the $(\bar{\sigma}, Q)$-plane. The trivial solution $\mathbf{X}_\circ$ of system (4.10), corresponding with $R_1 = 0$ and $R_2 = 0$, is stable inside interval $\bar{\sigma}_2 < \bar{\sigma} < \bar{\sigma}_1$ and it is unstable outside. The points $\bar{\sigma} = \bar{\sigma}_1$ and $\bar{\sigma} = \bar{\sigma}_2$ are Hopf bifurcation points of the trivial solution $\mathbf{X}_\circ$, see also Figure 11. In this case a stable periodic solution

emerges when the trivial solution $\mathbf{X}_o$ looses its stability. This stable periodic solution relates to the non-trivial fixed point $\mathbf{X_1}$ of system (4.12) which exists for $\bar{\sigma} > \bar{\sigma}_1$ or $\bar{\sigma} < \bar{\sigma}_2$. From equation (5.6) we have $\bar{\sigma}_{1,2} = \pm 0.107992$.

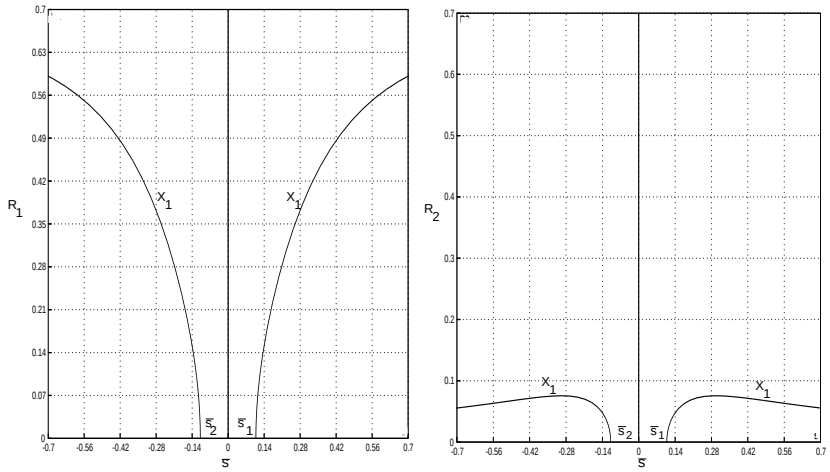

(a) (b)

FIGURE 11. The stable non-trivial fixed point $\mathbf{X_1}$ of system (4.12), corresponding with the stable periodic solution $\mathbf{X_1}$ of system (4.10), for Parameter set I, see Table 1, and $M = 0.2$ and $Q = 0.95$. (a) in the $(\bar{\sigma}, R_1)$-plane, (b) in the $(\bar{\sigma}, R_2)$-plane. Note $\bar{\sigma}_{1,2} = \pm 0.107992$

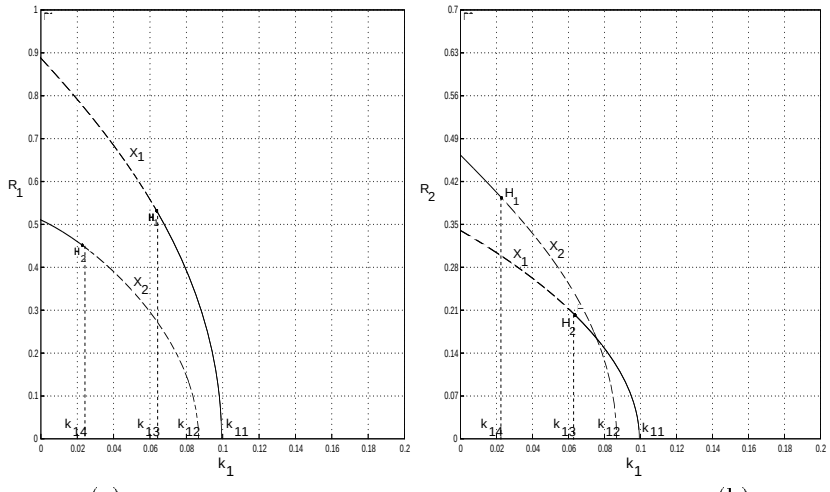

(a) (b)

FIGURE 12. The stability diagram of the non-trivial solution of system (4.12), for Parameter Set I (varied parameter κ_1, $M = 0.2$ and $Q = 0.95$), see Table 1. (a) in the (κ_1, R_1)-plane, (b) in the (κ_1, R_2)-plane. Note that $\kappa_{11} = 0.09936$, $\kappa_{12} = 0.08675$, $\kappa_{13} = 0.06367$, and $\kappa_{14} = 0.0228011$

As mentioned in section 5, interesting behavior such as the presence of a torus in system (4.10) happens when we vary the damping parameter κ_1 for fixed Q near 1. We show more completely the parameter diagram in the $(\kappa_1, \bar{\sigma})$-plane in Figure 10. This figure represents the parameter diagram of system (4.12) for Parameter Set I, $M = 0.2$, and $Q = 0.95$. The curves $\bar{\sigma}_1$ and $\bar{\sigma}_2$ are the existence boundaries of the fixed points $\mathbf{X_1}$ and $\mathbf{X_2}$ of system (4.12), respectively. The $\mathbf{X_i^+}$ indicates a stable non-trivial fixed point $\mathbf{X_i}$ and $\mathbf{X_i^-}$ indicates an unstable one, $\mathbf{i = 1, 2}$. The curves $CH_i, i = 1.2$ indicate Hopf bifurcation curves of the non-trivial fixed points $\mathbf{X_1}$ and $\mathbf{X_2}$, respectively. The point GH at $\kappa_1 = \kappa_1^* = 0.046897$ and $\bar{\sigma} = \bar{\sigma}^* = 0125067$ indicates an interchange point of the supercritical Hopf bifurcation and the subcritical Hopf bifurcation of the non-trivial fixed point $\mathbf{X_2}$. Note that for $\bar{\sigma} > \bar{\sigma}^*$ the bifurcation is subcritical, and it is a supercritical for $\bar{\sigma} < \bar{\sigma}^*$. The horizontal line $\bar{\sigma} = 0.1$ is an example of bifurcation path of the stability of the solutions of system 4.12. The curve CLP represents a limit point bifurcation curve of the periodic solutions **Ps** which appears via a Hopf bifurcation at curve CH_1. Crossing this curve the stable periodic solution **Ps** vanishes. Note that $\bar{\sigma}^2 = 0.07769$, $\bar{\sigma}^1 = 0.279403$, $\kappa_{11} = 0.09936$, $\kappa_{12} = 0.08675$, $\kappa_{13} = 0.06367$, and $\kappa_{14} = 0.0228011$.

In our numerical example, we vary the parameter κ_1 along line $\bar{\sigma} = 0.1$, see Figure 10 and 13. We find that a hyperbolic non-trivial fixed point $\mathbf{X_1}$ is stable in the interval $\kappa_{13} < \kappa_1 < \kappa_{11}$. Crossing the curve CH_1 at point H_1, it becomes unstable and a supercritical Hopf bifurcation takes place. Figure 12 (a) and (b) show the stability diagram of system (4.12) in the (κ_1, R_1)-plane and in the (κ_1, R_2)-plane, respectively. The non-trivial fixed point $\mathbf{X_2}$ is unstable in region $\mathrm{III_a}$ for $\kappa_{14} < \kappa_1 < \kappa_{12}$. It becomes stable when crossing the curve CH_2 and a supercritical Hopf bifurcation emerges at point H_2. A stable periodic solution **Ps** exists in the interval $\kappa_{14} < \kappa_1 < \kappa_{13}$.

In the full system (4.10), the non trivial fixed points of system (4.12) correspond with their periodic solutions. The stability diagram of the solutions is illustrated in Figure 13. We represent them in the κ_1-line for $\bar{\sigma} = 0.1$. The curves $\bar{\sigma}_i, i = 1, 2.$ are the Hopf bifurcation curves of the trivial solution $\mathbf{X_o}$.

We show the trivial solution $\mathbf{X_o}$ is stable for $\kappa_1 < \kappa_{11}$ and it undergoes Hopf bifurcation at $\kappa_1 = \kappa_{12}$. The stable periodic solution $\mathbf{X_1}$ emerges and changes its stability when it crosses the curve CH_1 at $\kappa_1 = \kappa_{13}$, see Figure 10. The curves $CH_i, i = 1, 2.$ relate to the Neimark-Sacker curves of system (4.10). We denote the Neimark-Sacker bifurcation points as $NS_i, i = 1.2$ which correspond with the Hopf bifurcation points $H_i, i = 1, 2.$ in Figure 10. We note that for increasing $\bar{\sigma}$ from a certain value, the Neimark-Sacker bifurcation of periodic solution $\mathbf{X_2}$ is subcritical. It becomes a supercritical bifurcation when $\bar{\sigma}$ is decreased and tends to zero.

When the stable periodic solution $\mathbf{X_1}$ looses its stability then a supercritical Neimark-Sacker bifurcation NS_1 appears at $\kappa_1 = \kappa_{13}$. The unstable periodic solution $\mathbf{X_2}$ appears when the trivial solution $\mathbf{X_o}$ is crossing the curve $\bar{\sigma}_2$. It becomes stable at $\kappa_1 = \kappa_{14}$. We find that a subcritical Neimark-Sacker bifurcation emerges at point NS_2 (point H_2 in Figure 10) for $\kappa_1 = \kappa_{14}$. A stable torus **T**, related to the stable periodic solution **Ps**, takes place for $\kappa_1 < \kappa_{13}$ and it disappears when κ_1 reaches κ_{14}. Note that for $\kappa_1 < \kappa_{14}$ we also have a stable periodic solution $\mathbf{X_2}$. We find that for $\kappa_1 < \kappa_{13}$ the amplitude R_1 of the periodic solution $\mathbf{X_1}$ is bigger than for the non-trivial solution $\mathbf{X_2}$, but the amplitude R_2 of the non-trivial $\mathbf{X_1}$ is less than for the periodic solution $\mathbf{X_2}$. Both R_1 and R_2 are increasing when κ_1 is decreasing. Note that $R_1 \to 0$ for $\kappa_1 \to \kappa_{13}^\star$ and $R_2 \to 0$ for $\kappa_1 \to \kappa_{14}^\star$, see Figure 13.

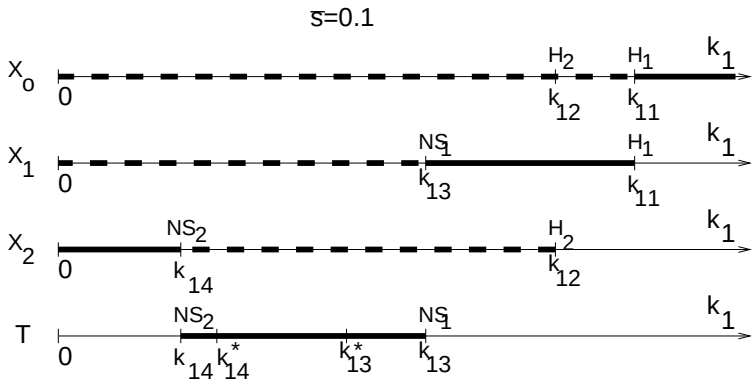

FIGURE 13. The Stability line of the trivial solution $\mathbf{X}_\circ$, the periodic solutions $\mathbf{X_1}$ and $\mathbf{X_2}$ and the torus $\mathbf{T}$ of the system (4.10) for varying κ_1 and Parameter Set I (see Table 1), $M = 0.2$, $Q = 0.95$, and $\bar{\sigma}_1 = 0.1$. The solid line indicates a stable solution and dashed line for unstable solution. Numerical calculation shown that $\kappa^\star_{13} = 0.0484171$, $\kappa^\star_{14} = 0.0287773$, and $\kappa^{4\star}_1 = 0.0280696$

.

9. The case M order ε

In applications we usually have to take the absorber mass (and so the mass ratio M) really small and the question rises whether we can still suppress or at least significantly reduce self-excited vibrations in this case. In [8] a numerical simulation is given which does not agree with the harmonic balance result of the authors. We shall show that this is caused by the necessity to rescale the parameter M with as a consequence that we have to take into account second order effects. We rescale $M = \varepsilon \bar{M}$.

In the case the mass ratio M is small; to avoid linear resonance we omit the case $Q \neq 1$. There are two possibilities to get a set of natural frequencies of the linearized system (3.7) without damping, Ω_1 and Ω_2, which depend on the value of Q, see equation (3.10). The possibilities are

$$\begin{cases} \text{for} \quad 1 < Q \\ \Omega_1 = 1 \quad \text{and} \quad \Omega_2 = Q \end{cases} \quad \text{or} \quad \begin{cases} \text{for} \quad 0 < Q < 1 \\ \Omega_1 = Q \quad \text{and} \quad \Omega_2 = 1 \end{cases}$$

The combination resonance takes place if $\eta_\circ = |\Omega_2 - \Omega_1|$.

To get a standard form (3.7), we use transformation (3.6) where now

$$\begin{cases} \text{for} \quad 1 < Q \\ a_1 = 0 \quad \text{and} \quad a_2 = \frac{Q^2-1}{Q^2} \end{cases} \quad \text{or} \quad \begin{cases} \text{for} \quad 0 < Q < 1 \\ a_1 = \frac{Q^2-1}{Q^2} \quad \text{and} \quad a_2 = 0 \end{cases}$$

After rescaling time by $\frac{1}{2(a_1-a_2)\eta_\circ{}^2}$, to second order (see [10]), the averaged system for the case $1 < Q$ is in the form

$$\begin{aligned} \dot{u_1} &= \varepsilon\left(-\bar{\kappa}_1\eta_\circ u_1 + (\alpha_{11} - 2Q\bar{\sigma})v_1 + Q_{13}v_2\right) + \varepsilon^2 G_1(u_1, v_1, u_2, v_2, \mu), \\ \dot{v_1} &= \varepsilon\left(-(\alpha_{11} - 2Q\bar{\sigma})u_1 - \bar{\kappa}_1\eta_\circ v_1 - Q_{13}u_2\right) + \varepsilon^2 G_2(u_1, v_1, u_2, v_2, \mu), \\ \dot{u_2} &= \varepsilon\left(-(\bar{\kappa}_2 - \bar{\beta}V^2)\eta_\circ u_2 + (\alpha_{13} - 2\bar{\sigma})v_2 + Cu_2(u_2^2 + v_2^2)\right) + \varepsilon^2 G_3(u_1, v_1, u_2, v_2, \mu), \\ \dot{v_2} &= \varepsilon\left(-(\alpha_{13} - 2\bar{\sigma})u_2 - (\bar{\kappa}_2 - \bar{\beta}V^2)\eta_\circ v_2 + Cv_2(u_2^2 + v_2^2)\right) + \varepsilon^2 G_4(u_1, v_1, u_2, v_2, \mu), \end{aligned} \tag{9.1}$$

where $\alpha_{11} = \frac{\bar{M}Q^2}{a_2\omega_1}$, $\alpha_{13} = \frac{\bar{M}Q^2(1-a_2)}{a_2\omega_2}$, $Q_{13} = \frac{(1-a_2)Q^2}{a_2}$, and $C = -\frac{3}{4}\Omega_2^2 B\eta_\circ a_2^2$ and

$$\begin{aligned}
G_1 &= A_1u_1 + A_2v_1 + A_3u_2 + A_4v_2 + A_5u_1(u_2^2+v_2^2) + A_6u_2(u_2^2+v_2^2)\\
G_2 &= -A_2u_1 + A_1v_1 - A_4u_2 + A_3v_2 + A_5v_1(u_2^2+v_2^2) + A_6v_2(u_2^2+v_2^2)\\
G_3 &= B_1v_1 + B_2u_2 + B_3v_2 + B_4u_2(u_2^2+v_2^2) + B_5v_2(u_2^2+v_2^2) + B_6v_2(u_2^2+v_2^2)^2\\
G_3 &= -B_1u_1 - B_3u_2 + B_2v_2 + B_4v_2(u_2^2+v_2^2) - B_5u_2(u_2^2+v_2^2) - B_6u_2(u_2^2+v_2^2)^2
\end{aligned}$$

see $(A.1)$ and $(A.2)$ in Appendix A for A_i and B_i for $i = 1..6$. We note that the system for the case $0 < Q < 1$ is obtained by transformation (3.6), with $\bar{x}_1 \to \bar{x}_2$ and $\bar{x}_2 \to \bar{x}_1$. This implies that system (9.1) is transformed by $u_i \to v_i$ and $v_i \to u_i$ for $i = 1, 2$ and exchanging Ω_1 and Ω_2, and conversely.

We find that to the lowest order in ε the trivial solution of the system (for both cases) is unstable. The eigenvalues of the trivial solution of system (9.1) are

$$\begin{aligned}
\lambda_{1,2} &= -\bar{\kappa}_1\eta_\circ \pm (\alpha_{11} - 2Q\bar{\sigma})i\\
\lambda_{3,4} &= (\bar{\beta}V^2 - \bar{\kappa}_2)\eta_\circ \pm (\alpha_{13} - 2\bar{\sigma})i
\end{aligned}$$

Note that, because of our assumption of the presence of self-excitation, we have $\bar{\beta}V^2 - \bar{\kappa}_2 > 0$. Using transformation to polar coordinates (4.11), we reduce system (9.1) to a three-dimensional system. It is now in the form

$$\begin{aligned}
\dot{R}_1 &= \varepsilon\left(-\bar{\kappa}_1\eta_\circ R_1 + Q_{13}R_2\sin(\psi)\right) + \varepsilon^2\bar{G}_1(R_1, R_2, \psi, \mu),\\
\dot{R}_2 &= \varepsilon\left(-(\bar{\kappa}_2 - \bar{\beta}V^2)\eta_\circ R_2 + CR_2^3\right) + \varepsilon^2\bar{G}_2(R_1, R_2, \psi, \mu),\\
\dot{\psi} &= \varepsilon\left(2(1-Q) + \bar{\sigma}\gamma_1 + Q_{13}R_2/R_1\cos(\psi)\right) + \varepsilon^2\bar{G}_3(R_1, R_2, \psi, \mu),
\end{aligned} \tag{9.2}$$

where a long but straightforward calculation produces

$$\begin{aligned}
\bar{G}_1 &= A_1R_1 + A_5R_1R_2^2 + A_4R_2\sin\psi + (A_6R_2^3 + A_3R_2)\cos\psi\\
\bar{G}_2 &= B_1R_1\sin\psi + B_2R_2 + B_4R_2^3\\
\bar{G}_3 &= A_2 + \frac{A_6R_2^3 + A_3R_2}{R_1}\sin\psi + \left(\frac{A_4R_2}{R_1} - \frac{B_1R_1}{R_2}\right)\cos\psi
\end{aligned}$$

$\gamma_1 = \alpha_{11} + \alpha_{13}$, R_1 and R_2 are bounded away from zero.

As C is negative, it is easy to see that up to first order in ε, $R_2 = \sqrt{-\frac{(\bar{\beta}V^2 - \bar{k}_2)\eta_\circ}{C}}$ corresponds with an invariant manifold. On this invariant manifold, system (9.2) has a fixed point $R_\circ = (R_{10}, R_{20}, \psi_0)$ corresponding with a periodic solution where $R_{10} = \frac{Q_{13}R_{20}}{\sqrt{\bar{\kappa}_1^2 + (2(1-Q) + \bar{\sigma}\gamma_1)}}$, $R_{20} = \sqrt{-\frac{(\bar{\beta}V^2 - \bar{k}_2)\eta_\circ}{C}}$, and $\psi_0 = \arccos(\frac{(2(Q-1) - \bar{\sigma}\gamma_1)R_{10}}{Q_{13}R_{20}})$. Note that Q_{13} is positive. To study the stability of this fixed point we check the characteristic equation of the linearization of system (9.2) at that point up to order ε. The characteristic equation is in the form

$$\lambda^3 + p\lambda^2 + q\lambda + r = 0.$$

We find that all the coefficients of the equation are positive and $pq - r > 0$, so that the fixed point $R_\circ$ is stable.

Figure 14 shows the maximum amplitude $R = \sqrt{R_{x_1}^2 + R_{x_2}^2}$ of the system (3.4) as a function of time t with the parameter set III for the numerical simulation as listed in Table 2.

Table 2: Parameter values for numerical examples.

Parameter	Set III
M	0.12
ε	0.1
κ_1	0.1
κ_2	0.1
β	0.1
V	$\sqrt{2.1}$
γ	4

As C is proportional to η_o, we note that to first order in ε the amplitude R_2 is independent of the parameter value η which means the absorber does not influences the vibration much. Adding the second order ε terms, we transform

$$R_1 = R_{10} + \varepsilon \bar{R}_1 \tag{9.3}$$

$$R_2 = R_{20} + \varepsilon \bar{R}_2 \tag{9.4}$$

$$\psi = \psi_0 + \varepsilon \bar{\psi} \tag{9.5}$$

yielding a system of the form

$$\begin{aligned} \dot{\bar{R}}_1 &= \varepsilon \left(C_1 \bar{R}_1 + C_2 \bar{R}_2 + C_3 \bar{\psi} + K_1 \right) + O(\varepsilon^2) \\ \dot{\bar{R}}_2 &= \varepsilon \left(C_4 \bar{R}_2 + K_2 \right) + O(\varepsilon^2) \\ \dot{\bar{\psi}} &= \varepsilon \left(C_5 \bar{R}_1 + C_6 \bar{R}_2 + C_7 \bar{\psi} + K_3 \right) + O(\varepsilon^2) \end{aligned} \tag{9.6}$$

where $K_i, i = 1, 2, 3$ are constants depending on R_{10}, R_{20}, and ψ_0, and so do the coefficients $C_i, i = 1..7$, see $A.3$ and $A.4$ in Appendix A. The fixed point of system (9.6) up to the lowest order of ε is $(\bar{R}_{1_0}, \bar{R}_{2_0}, \bar{\psi}_0)$, where $\bar{R}_{1_0}$, $\bar{R}_{2_0}$, and $\bar{\psi}_0$ are obtained by taking $\dot{\bar{R}}_1 = 0$, $\dot{\bar{R}}_2 = 0$ and $\dot{\bar{\psi}} = 0$, respectively.

Since $\bar{R}_{2_0}$ can be obtained explicitly, the amplitude of variable x_2 of system (3.4) can be given immediately. The expression is

$$R_{x_2} = |a_2| R_2 \tag{9.7}$$

This amplitude will reach the minimum value at

$$\bar{\sigma}_i = \frac{1}{3} \frac{(\pm 3\gamma_1 - \sqrt{3}\bar{\kappa_1}\eta_o)}{2(1-Q)} \tag{9.8}$$

In Figure 15 we show the maximum amplitude R_{x_2} of the system (3.4) with respect to parameter η and Q. (a). For the case $1 < Q$ and (b). for the case $0 < Q < 1$. Figure 16 illustrates the areas where the amplitude R_{x_2} can be reduced. For Parameter Set III, see Table 2, we show that inside the curves the amplitude R_{x_2} is suppressed. Figure 16.(a) is for the case $1 < Q$ and Figure 16.(b) for $0 < Q < 1$. We show that the minimum value at $\eta = 0.77607$ is 0.441621 for fixed $Q = 1.105$, see Figure 17.

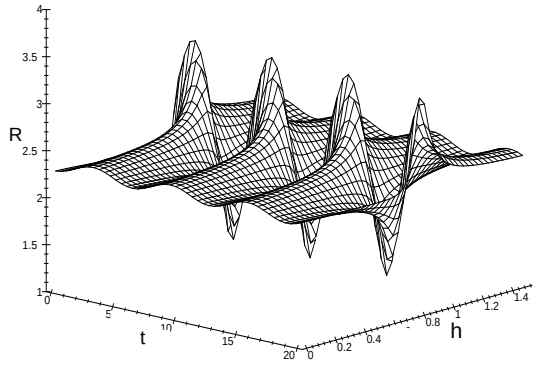

FIGURE 14. The maximum amplitude $R = \sqrt{R_{x_1}^2 + R_{x_2}^2}$ of system (3.4) to first order approximation for parameter Set III (see Table 2) and fixed $Q = 1.105$.

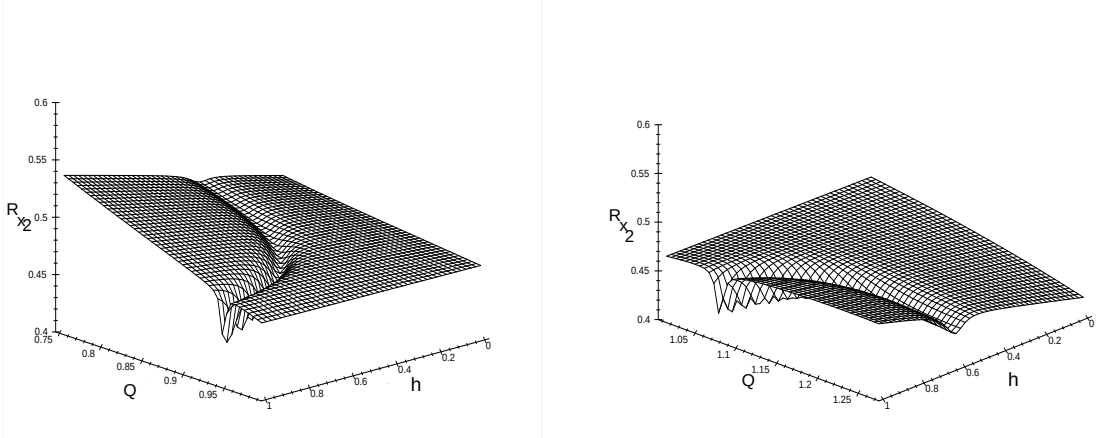

FIGURE 15. The maximum amplitude $R_{x_2} = |a_2|R_2$ of system (3.4) to second order approximation, for parameter set III (see Table 2). (a). For the case $1 < Q$ and (b). for the case $0 < Q < 1$.

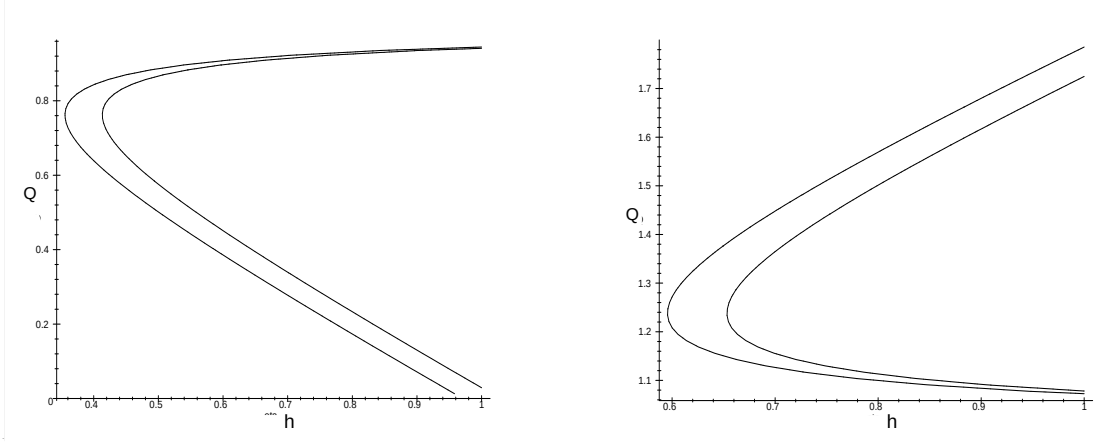

FIGURE 16. Diagram parameter (η, Q) for parameter Set III (see Table 2). Between the curves the maximum amplitude R_{x_2} can be reduced. (a). For the case $1 < Q$ and (b). for the case $0 < Q < 1$.

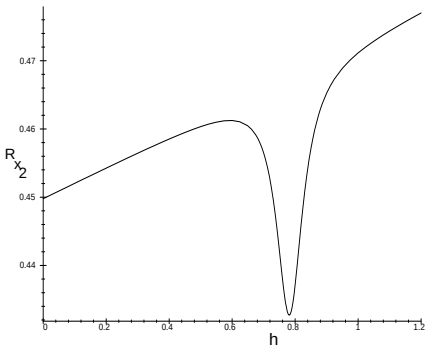

FIGURE 17. The maximum amplitude R_{x_2} of system (3.4) Parameter Set III (see Table 2) and fixed $Q = 1.105$. The minimum value can be reached at $\eta = 0.77607$ and $R_{x_2} = 0.441621$.

10. CONCLUSION

We have studied system (3.4), modeling flow-induced vibrations, by using the averaging method. There are two conditions needed for suppressing self excited vibrations. The first condition evaluates that the sum of the negative and the positive linear damping components determine the stability of certain modes and must be positive. The second condition is related to the parametric excitation frequency and determines, whether full quenching can be achieved or not in a certain interval. The presented results also demonstrate that a dynamic absorber

with parametric excitation is capable of enlarging the range of full vibration suppression near the combination resonance frequency.

The dynamics of the averaging system (4.10) is complex and it can be understood by the parameter diagram shown in Figure 10. By varying the parameter κ_1 we find equilibria, periodic solutions and torus solutions. The emergence of these solutions and their stability is tied in with Hopf and Neimark-Sacker bifurcations.

For applications the case of a small absorber mass (small M) is important. If M is of order ε the absorber influences the vibration in second order approximation. In Figure 16, we find the areas where the vibration is decreased. We can also calculate the minimum value that can be reached by the maximum amplitude of system (3.4) which shows that a large amount of quenching is still possible.

11. Acknowledgments

The authors wish to thank Prof. A. Tondl for formulating the problem.

The research was conducted in the department of Mathematics of the University of Utrecht; S.F was supported by a PGSM grant from Indonesia and CICAT TU Delft.

References

[1] H.Ecker, and A. Tondl, *Suppression of flow-induced vibrations by a dynamic absorber with parametric excitation.* Proc. of 7$^{\text{th}}$ International Conference on Flow-Induced Vibrations FIV2000, Lucerne, Switzerland, 2000.

[2] A. Tondl, *Quenching of Self-excited Vibrations*, Elsevier, Prague, 1991.

[3] A. Tondl, V. Kotek, and C.Kratochvil, *Vibration Quenching of Pendulum Type Systems by means of Absorber.*, CERM akademicke, Czech Republic, 2001.

[4] A. Tondl, *On the Interaction between Self-excited and Parametric Vibrations*, Monographs and Memoranda N0.25, National Research Institute for Machine Design, Prague, 1978.

[5] A. Tondl, *To the interaction of different types of excitations*, In *Proc.of Sem. Interactions and Feedback 97*, Prague, 25-26, 111-118, Prague, 1997.

[6] A. Tondl, *To the problem of quenching self-excited vibrations.*, Acta Technica CSAV 43, 109-116, 1998.

[7] A. Tondl, *The Method for Determination of Instability Intervals of Quasi-harmonic (parametric) System (in Czech)*, Aplikace matematiky, 4, N0.4, 278-289, 1959.

[8] A. Tondl, M. Ruijgrok, F. Verhulst, and R. Nabergoj, *Autoparametric Resonance in Mechanical Systems*, Cambridge University Press, New York, 2000.

[9] Y.A. Kuznetsov, *Elements of Applied Bifurcation Theory*, Second Edition, Springer, New York, 1997.

[10] J.A. Sanders, and F. Verhulst, *Averaging Methods in Nonlinear Dynamical Systems*, Appl.math. Sciences 59, Springer-Verlag, New York, 1985.

Appendix A. The second order approximation of Averaging System

The expressions for the coefficients of the second order approximation of system (9.1):

(A.1)

$$
\begin{aligned}
A_1 &= -\frac{\alpha_{11}\eta_\circ\theta_{12}}{\omega_1+\omega_2} - \theta_{13}\eta_\circ + 2\theta_{11}\bar{\sigma}\\
A_2 &= -\frac{1}{4}\frac{(\alpha_{11}+\bar{\sigma}\alpha_{12}\omega_1)^2}{\omega_1^3} - \frac{1}{4}\frac{\theta_{11}^2\eta_\circ^2}{\omega_1} + \frac{\alpha_{11}\alpha_{13}}{\omega_1(\omega_1+\omega_2)} - \frac{1}{2}\frac{Q_{11}^2}{(4\omega_1^2-1)\omega_1} - 2\frac{\alpha_{11}\bar{\sigma}}{\omega_1\eta_\circ}\\
A_3 &= -\frac{1}{2}\frac{\eta_\circ\omega_2 Q_{11}\theta_{12}}{\omega_1(\omega_1+\omega_2)} - \frac{1}{8}\eta_\circ\left(\frac{\theta_{11}Q_{12}}{\omega_1^2} - \frac{\theta_{22}Q_{12}}{\omega_1\omega_2}\right)\\
A_4 &= -\frac{1}{8}\frac{Q_{12}\alpha_{12}\bar{\sigma}}{\omega_1^2} + \frac{1}{4}\frac{Q_{12}\bar{\sigma}}{\omega_1\omega_2} - \frac{1}{8}\frac{Q_{12}\alpha_{11}}{\omega_1^3} + \frac{1}{8}\frac{\alpha_{13}Q_{12}}{\omega_1\omega_2^2} + \frac{1}{2}\frac{\alpha_{13}Q_{11}}{\omega_1(\omega_1+\omega_2)} + \frac{1}{2}\frac{\alpha_{13}}{\omega_1} - \frac{Q_{12}\bar{\sigma}}{\omega_1\eta_\circ}\\
A_5 &= \frac{3}{2}\frac{\alpha_{11}\omega_2^2 B\eta_\circ^3}{\omega_1+\omega_2}\\
A_6 &= \frac{3}{32}\frac{Q_{12}\omega_2 B\eta_\circ^3}{\omega_1} + \frac{3}{8}\frac{Q_{11}\omega_2^3 B\eta_\circ^3}{\omega_1(\omega_1+\omega_2)}
\end{aligned}
$$

(A.2)

$$
\begin{aligned}
B_1 &= -\frac{1}{2}\frac{\alpha_{11}Q_{11}}{\omega_2(\omega_1+\omega_2)} - \frac{1}{2}\frac{\alpha_{11}}{\omega_2}\\
B_2 &= \frac{\alpha_{11}\theta_{12}\eta_\circ}{\omega_1+\omega_2} + 4\theta_{22}\bar{\sigma} + 2\theta_{14}\eta_\circ\\
B_3 &= -\frac{(\omega_2\bar{\sigma}+\alpha_{13})\bar{\sigma}}{\omega_2^2} - \frac{\alpha_{11}\alpha_{13}}{\omega_2(\omega_1+\omega_2)} - \frac{1}{4}\frac{\theta_{22}^2\eta_\circ^2}{\omega_2} - \frac{1}{4}\frac{\alpha_{13}^2}{\omega_2^3} + 2\frac{\alpha_{13}\bar{\sigma}}{\omega_2\eta_\circ}\\
B_4 &= -\frac{3}{4}\frac{\alpha_{11}\omega_2^2 B\eta_\circ^3}{\omega_1+\omega_2} - \frac{3}{8}(-2\omega_2\bar{\sigma}+\alpha_{13})B\eta_\circ^3 + \frac{3}{4}\alpha_{13}B\eta_\circ^3 + 3\omega_2^2 B\eta_\circ^2\bar{\sigma}\\
B_5 &= -\frac{3}{8}\theta_{22}\omega_2 B\eta_\circ^4\\
B_6 &= -\frac{27}{128}\omega_2^3 B^2\eta_\circ^6
\end{aligned}
$$

where $\alpha_{12} = -2Q$, $Q_{11} = Q^2$, $Q_{12} = (1-a_2)Q^2$, $\theta_{11} = \bar{\kappa}_1$, $\theta_{12} = \bar{\kappa}_1(1-a_2) - (\bar{\kappa}_2 - \bar{\beta}V^2)$, $\theta_{13} = \bar{M}\bar{\kappa}_1$, $\theta_{14} = \bar{M}\bar{\kappa}_1(1-a_2)$, and $\theta_{22} = \bar{\kappa}_2 - \bar{\beta}V^2$.

The expressions for the coefficients of the second order approximation of system (9.6):

$$
\begin{aligned}
C_1 &= -\bar{\kappa}_1 \eta_\circ \\
C_2 &= \frac{1}{2\omega_1} Q_{12} \sin\psi_0 \\
C_3 &= \frac{1}{2\omega_1} Q_{12} R_{20} \cos\psi_0 \\
C_4 &= -\frac{9}{4} R_{20}^2 a_2^2 \omega_2^2 B \eta_\circ^3 - \theta_{22} \eta_\circ \\
C_5 &= -\frac{1}{2} \frac{Q_{12} R_{20} \cos\psi_0}{R_{10}^2 \omega_1} \\
C_6 &= \frac{1}{2} \frac{Q_{12} \cos\psi_0}{R_{10} \omega_1} \\
C_7 &= -\frac{1}{2} \frac{Q_{12} R_{20} \sin\psi_0}{R_{10} \omega_1}
\end{aligned}
\tag{A.3}
$$

(A.4)

$$K_1 = (A_3 R_{20} + A_6 R_{20}^3)\cos\psi_0 + A_4 R_{20} \sin\psi_0 + R_{10} A_1 + A_5 R_{10} R_{20}^2$$

$$K_2 = B_1 R_{10} \sin\psi_0 + B_2 R_{20} + B_4 R_{20}^3$$

$$K_3 = \left(\frac{A_4 R_{20}}{R_{10}} - \frac{B_1 R_{10}}{R_{20}}\right) cos\psi_0 + \left(\frac{A_3 R_{20}}{R_{10}} + \frac{A_6 R_{20}^3}{R_{10}}\right) \sin\psi_0 + A_2 - B_3 - B_5 R_{20}^2 - B_6 R_{20}^4$$